ORIGINAL RESEARCH **Open access**

Optimized Sliding Mode Control of Photovoltaic Boost Converters Using GA in an IoT Framework

Erik Van der Meer[1*], Lieke Jansen[1], Bram de Vries[2]

Abstract

This study introduces an innovative optimization approach for boost converter controllers by adjusting the voltage and current regulation mechanisms in Photovoltaic (PV) systems, specifically utilizing either Sliding Mode Control (SMC) or Sliding Mode plus Proportional-Integrative Control (SMPIC). The optimization leverages a Genetic Algorithm (GA) within an Internet of Things (IoT) framework. The cloud server executes the GA, which is subsequently used to tune the SMC and SMPIC parameters for the PV plant's boost converter. The data exchange between the IoT-enabled PV plant and the cloud server involves transmitting measured PV voltages and currents to the server. At the same time, the optimized controller parameters are sent back to the plant. Telemetry data from the IoT system is utilized to compute the fitness function of specific solutions, effectively applying machine learning to model the solar plant. Hardware-based experimental tests are conducted to assess system performance. A comparative analysis between deterministic and heuristically derived parameters for SMC and SMPIC demonstrates significant improvements, particularly in minimizing overshoot and reducing settling time.

Keywords Genetic algorithm, Photovoltaic, Boost converter, Maximum power point tracking, Sliding mode control

*Correspondence:
Erik Van der Meer
e.vandermeer@tudelft.nl
[1] Department of Intelligent Energy Distribution Networks, Faculty of Electrical Engineering, Delft University of Technology, Delft, Netherlands
[2] Department of Artificial Intelligence for Power Systems, Faculty of Engineering, Eindhoven University of Technology, Eindhoven, Netherlands

Introduction

Environmental factors, particularly module temperature and solar irradiation, directly dictate the efficiency of PV power generation. Consequently, optimizing energy extraction from a PV system necessitates an algorithm capable of identifying the solar panel's peak operating threshold, commonly referred to as Maximum Power Point Tracking (MPPT) [1]. Furthermore, MPPT performance can be enhanced by analyzing the transient response of the underlying controllers—specifically, their capacity to sustain a targeted output against a reference and react to abrupt environmental shifts. The existing literature details various linear control strategies, including proportional-integral (PI), lead-lag [2], and state feedback systems [3]. Because the voltage-current relationship of a PV module exhibits significant nonlinearity dictated by technical constraints and atmospheric conditions, nonlinear controllers are also frequently employed. These are often integrated with advanced control frameworks, such as Fuzzy Logic [4], nonlinear-adaptive systems [5], standard adaptive controllers [6], finite control set model predictive control [7, 8], neural networks [9], and sliding mode control (SMC) [10].

For PV energy applications, SMC offers distinct advantages over alternative nonlinear methods, primarily due to its straightforward mathematical formulation and implementation. Moreover, SMC is frequently combined with other proven methodologies, including smooth switching functions and higher-order sliding surfaces (HOSS) featuring integral action.

This is an open access article distributed under the terms of the Creative Commons Attribution-NonCommercial-ShareAlike 4.0 International License (CC BY-NC-SA 4.0), which permits non-commercial use, distribution, reproduction, and adaptation in any medium or format, provided that appropriate credit is given to the original author(s) and source, a link to the license is provided, and any changes made are indicated. Adapted material must be distributed under the same license.

© 2024 The Author(s). | Published by Institute of Smart Energy Systems Press

These hybrid approaches have demonstrated high accuracy and robustness both in computational simulations and physical bench testing [11].

Optimization research aims to identify the most effective configuration for a given controller. As a robust instrument in controller design, these methods attempt to determine parameter values that minimize an objective function while adhering to specific constraints [12]. The Genetic Algorithm (GA), initially formulated by Holland [13], is a heuristic, adaptive search technique. Rooted in the principles of Darwinian natural selection, GA is widely utilized in both general research and machine learning to address complex optimization challenges that would otherwise be computationally prohibitive to solve using traditional means [14].

In previous work by Wang *et al*. [15], a GA was utilized to tune the parameters of a neural network-driven Proportional-Integral-Derivative (PID) controller for a boost converter, contrasting the optimized outcomes against non-optimized performance. Computational simulations of the GA-derived plant parameters revealed diminished overshoot and accelerated settling times compared to the baseline, unoptimized controller. A parallel investigation applying this methodology to a buck converter was documented in Sivamani *et al*. [16].

An alternative optimization strategy for PV system boost converters was explored in Vargas Gil *et al*. [10], which applied a Weighted-Particle Swarm Optimization (w-PSO) to calibrate a Sliding Mode plus PI controller. The system was initially modeled using an AC small-signal approach to establish the Sliding Mode Control law. Subsequently, w-PSO was deployed to derive the ideal parameters via simulation, which were then validated on a physical boost converter prototype.

Nevertheless, most optimization procedures are executed in simulation environments before physical implementation. This approach inherently suffers from approximation errors, rounding discrepancies, and modeling constraints. Consequently, exploiting network connectivity offers a compelling alternative for real-time monitoring, data acquisition, and direct optimization of the solar facility.

The IoT comprises an interconnected web of devices, ranging from basic sensors to advanced smart equipment [17]. With the rapid expansion of IoT technologies, leveraging network capabilities specifically for solar power applications has become increasingly feasible. By facilitating automation and control, IoT serves as the foundation of modern electronic systems. This connectivity taps into the vast data generated by the plant and extends to industrial and machinery processes [18]. IoT infrastructures provide facilities with new analytical tools and data to improve optimization. Telemetry enables the integration of real-time operational data and diagnostics, ultimately lowering operating expenses, extending equipment longevity, and allowing for tailored performance. Through wired or wireless channels, devices exchange critical information for monitoring, logging, and decision-making, culminating in an autonomous network of intelligent assets.

Within this framework, research presented in Rouibah *et al*. [19] describes an IoT-enabled PV system utilizing ESP and Arduino microcontrollers to track and broadcast metrics such as duty cycle, PV voltage, PV current, load voltage, and load current online. While the study implemented standard tracking algorithms and yielded stable outcomes, the low-cost nature of the project resulted in suboptimal overall performance. Similar methodologies focusing on voltage and current monitoring have been documented in Banu and Moses [20], Rouibah *et al*. [21], and Rokonuzzaman *et al.* [22].

Furthermore, Habib *et al*. [23] demonstrated improved voltage profiles across various load nodes and mitigated transmission line power losses. Relying on an IoT architecture and a mathematical system model, an optimization algorithm was employed to determine the ideal real-time reactive power setpoint for individual plants using transmitted data. This approach successfully improved the overall voltage profiles at load buses by up to 68%.

Accordingly, this paper introduces an adaptive heuristic search algorithm designed to determine the optimal parameters for the controllers previously developed by the authors in SMC [11] and SMPIC [10]. The established mathematical models for both control strategies are thoroughly detailed in those prior publications. Unlike earlier studies [2, 10, 15, 16]

© 2024 The Author(s). | Published by Institute of Smart Energy Systems Press

where heuristic searches were performed in simulation before prototype application, this research diverges from that workflow. Instead, it exploits IoT capabilities to identify controller parameters during runtime. A cloud-based server evaluates the GA using empirical data transmitted via an internet connection. Data is obtained from tests performed directly on a physical prototype utilizing real components. By utilizing empirical data, mathematical modeling approximations are eliminated, allowing the system to operate with pre-optimized controllers and ultimately yielding tangible enhancements in overall system performance.

Topology

This section details the architecture of the PV system, which consists of a PV panel feeding into a boost converter governed by either SMC [11] or SMPIC [10], alongside an inverter responsible for direct current-to-alternating current (DC/AC) conversion. Furthermore, it describes the network infrastructure enabling the PV system to link with a cloud server over Ethernet. This server executes the GA for continuous monitoring and eventual controller reconfiguration. The complete system topology is illustrated in **Figure 1.**

© 2024 The Author(s). | Published by Institute of Smart Energy Systems Press

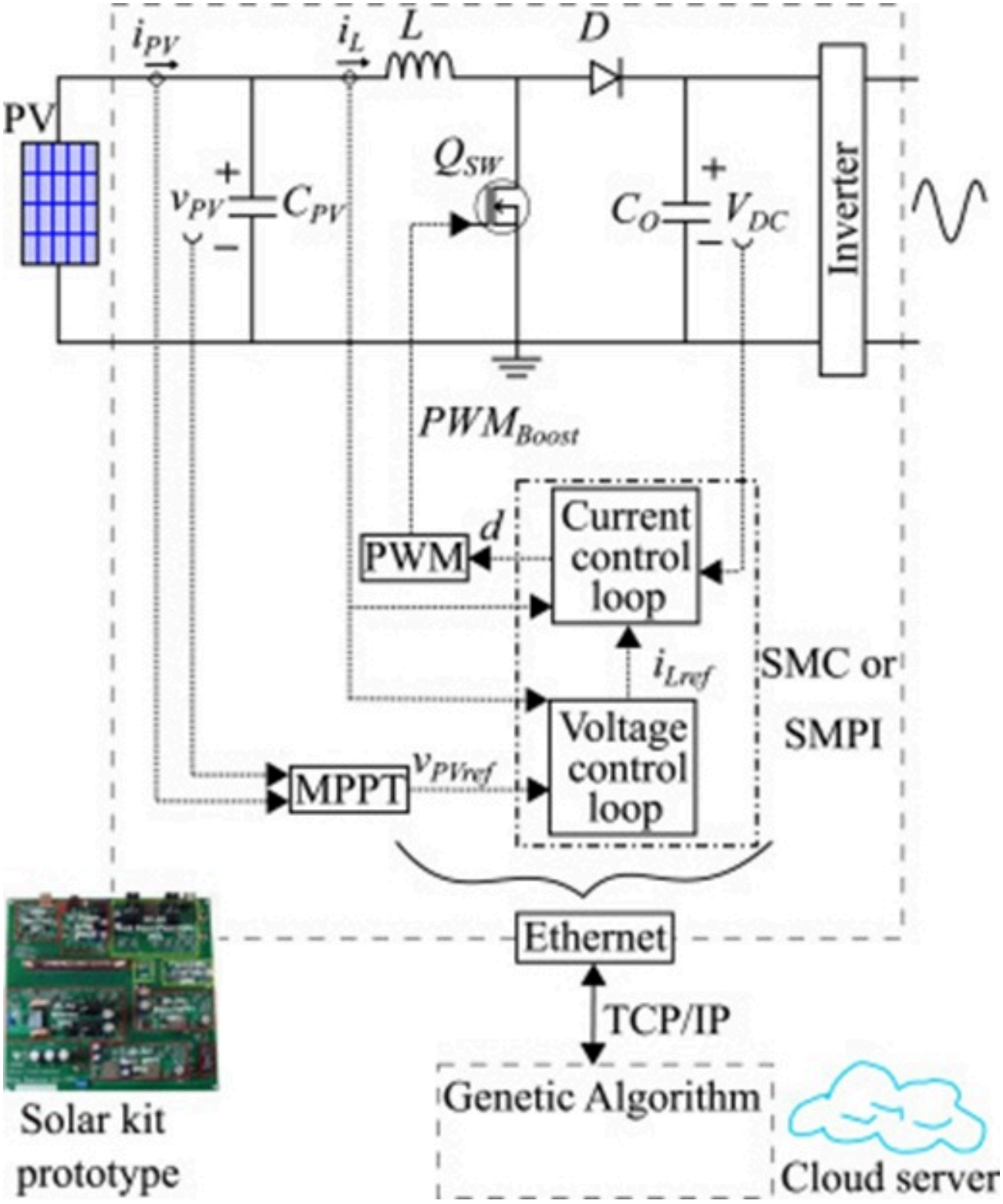


Figure 1. Block diagram of PV system.

Boost converter

© 2024 The Author(s). | Published by Institute of Smart Energy Systems Press

The boost converter elevates and stabilizes the PV panel voltage vPV to meet the specific requirements of the downstream system connected to its output (VDC), such as an inverter, based on the designated application, as depicted in **Figure 1.**

The input voltage (vPV) and inductor current (iL) of the boost converter are regulated using a constant switching frequency signal (Pulse-Width Modulation - $PWMBoost$), which dictates the on or off states of the MOSFET (QSW). As indicated in the block diagram, the control architecture is split into two distinct loops: The MPPT algorithm supplies the reference voltage (vPVref) to the outer voltage control loop. This stage adjusts the DC component of vPV to match its setpoint, thereby providing an inductor current reference ($iLref$) to the inner current control loop. Subsequently, the inner current control loop evaluates iL and produces a corresponding duty cycle (d) via a $PWMBoost$ applied to QSW.

During the period when QSW is switched on, the reverse-biased diode (D) isolates the output stage. Consequently, the inductor (L) is grounded, allowing current to pass through and accumulate energy [24]. Conversely, when QSW is switched off, the energy previously stored in L, combined with the energy from the input capacitor (CPV), propagates through D toward VDC. To maintain a steady output voltage, the output capacitor (CO) is assumed to be sufficiently large [25].

Mathematical model

An equivalent linear circuit model is established by linearizing the PV module along a straight line tangent to its current-voltage (I-V) curve at the specific operating point [26].

When the switch QSW is closed, the dynamic equations representing the circuit's state are derived by calculating the derivatives of the capacitor voltage and the inductor current:

$$\begin{cases} \dfrac{di_L}{dt} = \dfrac{v_{PV}(t)}{L} \\ \dfrac{dv_{PV}(t)}{dt} = \dfrac{V_{eq} - v_{PV}(t)}{R_{eq}C_{PV}} - \dfrac{i_L(t)}{C_{PV}}, \end{cases} \quad (1)$$

In this context, Veq represents the linearized voltage of the PV panel, and Req denotes the linearized resistance of the panel [27].

Conversely, the dynamic equations when QSW remains open are expressed as follows:

$$\begin{cases} \dfrac{di_L(t)}{dt} = \dfrac{v_{PV}(t) - V_{DC}}{L} \\ \dfrac{dv_{PV}(t)}{dt} = \dfrac{V_{eq} - v_{PV}(t)}{R_{eq}C_{PV}} - \dfrac{i_L(t)}{C_{PV}}. \end{cases} \quad (2)$$

Sliding Mode Plus PI Control (SMPIC)

The system's control objectives focus on the discrepancy between the reference value and the measured variable, as the primary goal of the control strategy is to drive this error to zero. Consequently, the sliding surface is formulated based on the voltage error and the current error.

To enhance the controller's dynamic response, however, the derivatives of these errors (ev and ei) are incorporated, resulting in two second-order sliding surfaces:

© 2024 The Author(s). | Published by Institute of Smart Energy Systems Press

$$\sigma = \begin{bmatrix} \sigma_1 \\ \sigma_2 \end{bmatrix} = \begin{bmatrix} e_v + k_v \frac{de_v}{dt} \\ e_i + k_i \frac{de_i}{dt} \end{bmatrix} = 0, \quad (3)$$

Here, the constants kv and ki are selected based on the targeted system dynamics.

The switching of the sliding variable σ is governed by the S(x) function, which simultaneously dictates how the system reacts to fluctuations in state variables. The S(x) function works by bounding the surface when it reaches its maximum or minimum thresholds. Furthermore, owing to its linear characteristics, it effectively mitigates chattering as the system state approaches the switching surface [28], according to the following definition:

$$S(x) = \begin{cases} 1 & \text{if } x > 1 \\ x & \text{if } -1 \le x \le 1 \\ -1 & \text{if } x < -1 . \end{cases} \quad (4)$$

The control laws governing both control loops are established as follows [10]:

$$i_{Lref} = (k_{pv} + \frac{k_{iv}}{s}) S(\sigma_1) \quad (5)$$

And:

$$d = (k_{pc} + \frac{k_{ic}}{s}) S(\sigma_2), \quad (6)$$

Where kpv, kiv, kpc, and kic represent the PI controller gains.

Sliding Mode Control (SMC)

Current control loop

By employing a First Order Sliding Mode Control alongside a First Order Sliding Surface, **Eqs. 1 and 2** can be reformulated as:

$$\frac{di_L(t)}{dt} = \frac{1}{L} \frac{2v_{PV}(t) - V_{DC}}{2} + \frac{1}{L} \frac{V_{DC}}{2} \text{sign}(\sigma_I), \quad (7)$$

Where $\sigma I = iLref - iL$.

To enhance the dynamic behavior—and specifically to eradicate the steady-state error introduced by the application of the soft switching function **Eq. 4**—an integrative second-order sliding surface can be implemented [29]:

$$\sigma_i = \int \lambda(e_i) e_i dt + e_i = 0, \quad (8)$$

In this expression, σi represents the sliding variable, ei = $iLref$ -, and (ei) denotes a function required to fulfill the system's attractiveness condition, as detailed in Inomoto *et al*. [11]. Consequently, the current controller is given by:

© 2024 The Author(s). | Published by Institute of Smart Energy Systems Press

$$d = \frac{S(k_i\sigma_i) + 1}{2}, \quad (9)$$

Where $ki > 0$, which can be selected arbitrarily to balance rapid response times against the minimization of chattering.

Voltage control loop

An integrative second-order sliding surface is similarly selected for the voltage control loop:

$$\sigma_v = \int \lambda(e_v)e_v dt + e_v = 0, \quad (10)$$

Where σv serves as the sliding variable, $ev = vPVref - vPV$, and (ev) is a function strictly satisfying the system's attractiveness condition.

As a result, the voltage loop controller takes the form:

$$i_{Lref} = I_{MAX}\frac{1 - S(k_v\sigma_v)}{2}, \quad (11)$$

Here, $IMAX$ signifies the peak permissible current for the hardware components, while kv corresponds to ki in **Eq. 9,** acting as the coefficient for the smooth switching function.

Genetic Algorithm - GA

Advancements in robust hardware and software methodologies enable the continuous monitoring, reconfiguration, and fault detection of complex systems. These methodologies are often categorized under machine learning or deep learning. The integration of the Genetic Algorithm (GA), the Internet of Things (IoT), and big data analytics (BDA) has progressed significantly toward plant automation. The primary goal of these technologies is to create intelligent, autonomous, and innovative condition-monitoring frameworks that facilitate accurate failure detection and classification, alongside smart decision-making capabilities for immediate plant interventions [30].

© 2024 The Author(s). | Published by Institute of Smart Energy Systems Press

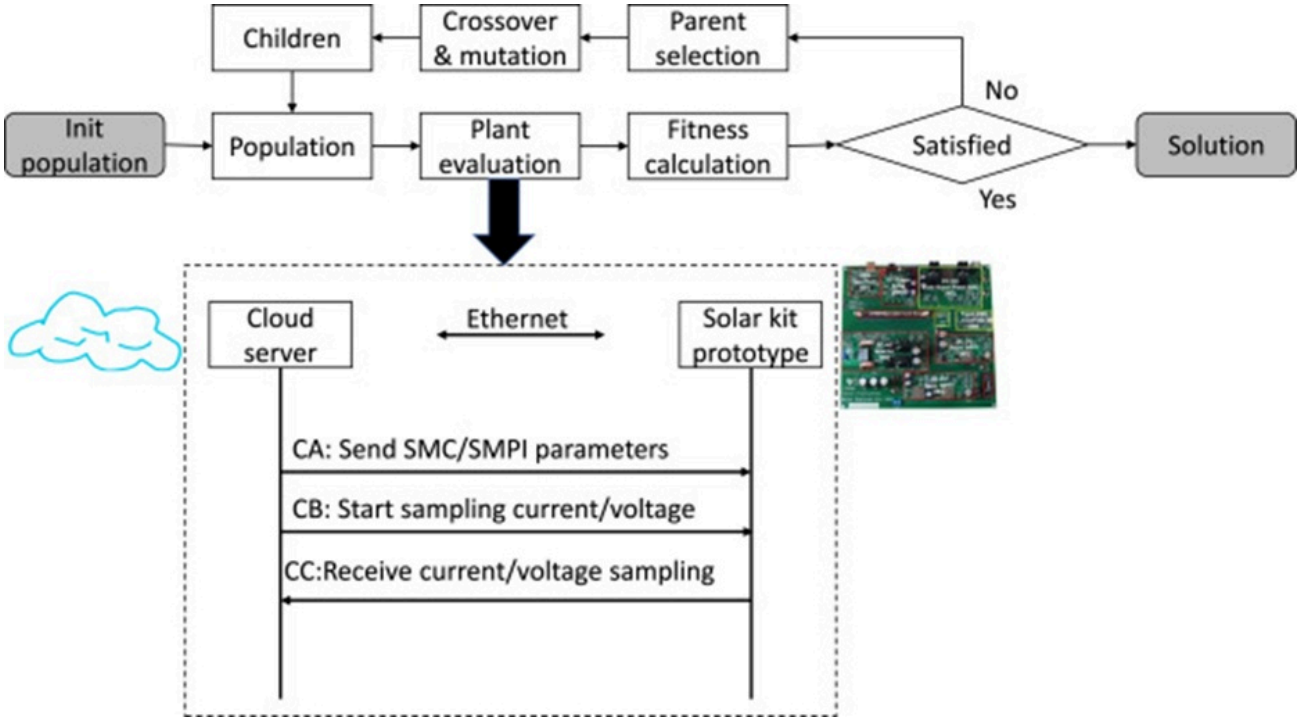


Figure 2. GA algorithm.

This section outlines the deployment of the GA within the cloud server framework of the proposed study; the corresponding GA flowchart is illustrated in **Figure 2**. The GA initiates with a predefined problem. Subsequently, the plant undergoes real-time evaluation and is assigned a fitness value, thereby assessing the viability of a potential solution. If the predefined criteria are not met, the population undergoes mutation and recombination—mirroring natural genetics—to generate new offspring. This iterative cycle spans multiple generations. Therefore, it progressively cultivates superior individuals until the targeted condition is satisfied [31]. The introduced GA operates across an IoT infrastructure that pairs a cloud server with a physical solar plant prototype. Via network communication, the cloud server transmits the SMC/SMPIC parameters to the physical plant while instantaneously receiving acquired current and voltage data. The solar prototype is equipped with essential overcurrent and overvoltage safeguards to ensure secure system operation.

Initial population

The algorithm initializes the population by generating N random parents, which serve as potential candidate solutions. In this context, a chromosome represents a single complete solution to the problem at hand, while a gene denotes an individual element's position within that chromosome.

Fitness function

Following the creation of the initial population, the performance of each member is evaluated via an adaptive function. This process assigns a fitness value to every candidate solution, acting as a metric of its overall quality [14]. In the context of the proposed topology, settling time and overshoot serve as the primary quality criteria. Defining these parameters is critical, as the GA relies heavily on this information to select the optimal solution for the final population.

Because the proposed PV system topology utilizes two distinct controllers (for the current control loop and the voltage control loop), the fitness function is formulated as follows:

© 2024 The Author(s). | Published by Institute of Smart Energy Systems Press

$$ITAE = \int_0^\tau t|e(t)|\,dt \quad (12)$$

And:

$$ISE = \int_0^\tau e^2(t)\,dt, \quad (13)$$

The first equation is beneficial for minimizing the persistent error over time, whereas the second is effective in mitigating substantial transient errors. By employing these two equations, the PV system is projected to achieve minimal overshoot alongside low steady-state oscillations [10]. Consequently, during the optimization process for both controllers, a lower fitness result indicates superior performance.

Parent selection

Parent selection constitutes the mechanism by which individuals are chosen for recombination to produce offspring for the subsequent generation. Maintaining an adequate degree of diversity among parents is crucial to prevent premature convergence. Common techniques for this stage include Proportionate Roulette Wheel Selection, Linear Ranking Selection, Exponential Rank Selection, and Tournament Selection. Literature suggests that Tournament Selection offers efficient convergence, straightforward implementation, and reduced susceptibility to dominance by overly fit individuals [31, 32].

Despite these advantages, the present study conducted a comparative analysis between Tournament Selection and Proportionate Roulette Wheel Selection. The latter was ultimately chosen because it can identify the optimal solution more rapidly.

Proportionate Roulette Wheel Selection assigns a higher probability weight to chromosomes based on their fitness scores, effectively “spinning” a virtual roulette wheel to determine the selected parent [33].

This virtual roulette wheel spin is mathematically represented by **Eq. 14.** Because a lower fitness score denotes a better solution, a correspondingly higher weight is assigned to those superior parents.

$$\text{parent} = \text{randsample}(W_1, ..W_n), \sum_{i=1}^{n} W_i = 1 \quad (14)$$

Where randsample represents a randomly generated number simulating the roulette wheel, and Wi denotes the ith weight.

Crossover and mutation

Crossover serves as a genetic operator designed to blend information from chosen parents, generating superior offspring for the subsequent generation [14]. In this context, the mathematical representations of both parents and children are floating-point numbers. Consequently, adhering to GA naming conventions, the chromosome representation in this study utilizes the IEEE 754 single-precision binary floating-point standard [34], as expressed by **Eq. 15**. A floating-point value is

© 2024 The Author(s). | Published by Institute of Smart Energy Systems Press

mapped into a 32-gene (bit) chromosome. Genes are randomly selected from both parents to combine their genetic information, thereby producing a novel chromosome. Occasionally, mutation occurs, which flips the value of one of the 32 genes (16). Mutation ensures population diversity; essentially, it prevents the algorithm from getting trapped in local optima while searching for the global optimal solution [35]. Following the mutation process, the 32-bit chromosome is converted back into a floating-point number:

$$\text{float} = s.2^{(128-e)}.m\,, \quad (15)$$

$$\text{mutation} = \text{bit}_p.q\,, \quad (16)$$

Where s is the sign; e is the exponent; m is the mantissa; p is a random number ∈ ℕ = {0, ..., 31}; q is a random number ∈ ℕ = {0, 1}.

Hardware Experimental Verification

The purpose of this research is to demonstrate the feasibility of applying the IoT framework for machine learning via GA to optimize SMPIC or SMC solar plant controllers. IoT offers multiple benefits, including the automation and monitoring of power generated by the solar plant, as well as system diagnostics.

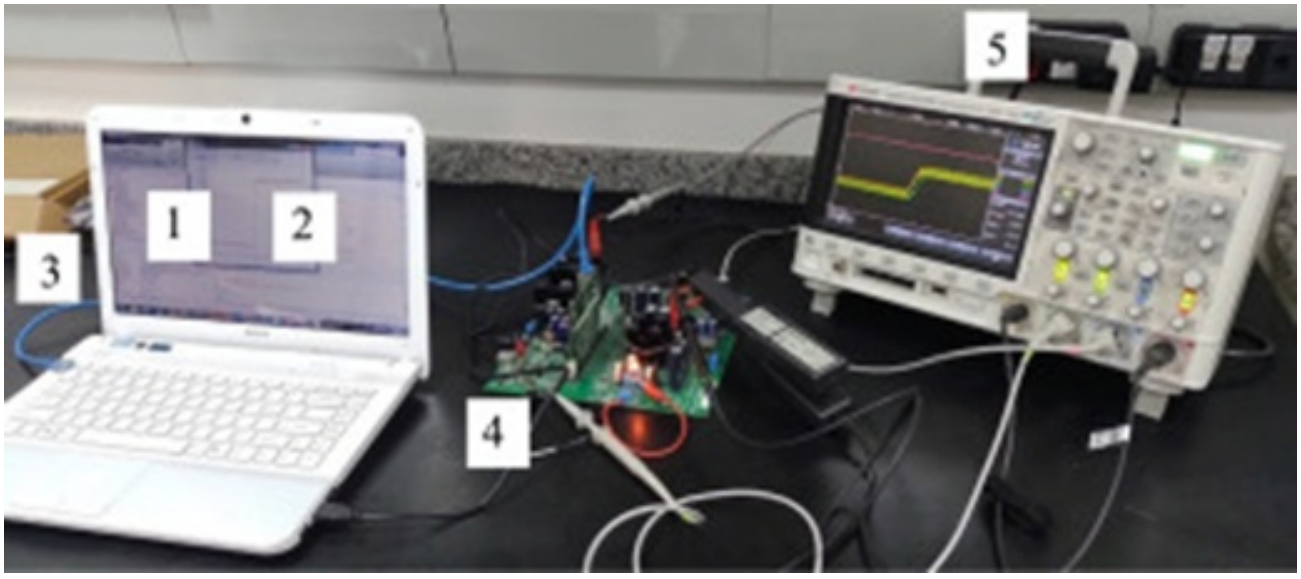


Figure 3. Experimental bench setup: (1) Code Composer Studio (CCS), (2) MATLAB, (3) Ethernet cable, (4) Solar Explorer Kit (TMDSSOLARCEXPKIT), and (5) Oscilloscope.

This study utilizes the Texas Instruments Solar Explorer Kit (TMDSSOLARCEXPKIT) equipped with a Digital Signal Processor (DSP) F28M35H52C [36]. As illustrated in **Figure 3**, this kit offers a low-voltage testbed featuring a PV array/module emulator designed for laboratory environments [37], alongside a buck-boost converter, a boost converter, a single-phase full-bridge inverter, and an Ethernet interface.

The PV emulator, which mimics the nonlinear I-V characteristics of a PV module across various irradiance levels **(Table 1)**, powers the boost converter input. The converter's output voltage is stabilized at approximately 30 V by the output boost capacitor and the single-phase inverter. The boost converter specifications are outlined in **Table 2.**

© 2024 The Author(s). | Published by Institute of Smart Energy Systems Press

DSP programming is executed in C using the Texas Instruments Code Composer Studio environment, which compiles a binary file that is subsequently uploaded via a USB connection. The DSP features a dual-core architecture: one core is dedicated to real-time control operations, while the ARM Cortex M3 processor handles communication tasks, including Ethernet networking. The real-time control processor is tasked with managing power electronic components such as the inverter and boost converter.

Table 1. Operating point at maximum power of the TMDSSOLARCEXPKIT [36].

Irradiance (W/m^2)	I_{PV_MPPT} (A)	V_{PV_MPPT} (V)	P_{max} (W)
1000	1.951	18.46	36.02
900	1.975	16.42	32.42
800	1.963	14.68	28.82
700	1.975	12.77	25.22
600	1.969	10.98	21.61
500	1.98	9.093	18.01
400	1.957	7.363	14.41
300	1.975	5.473	10.81
200	1.963	3.67	7.205

Table 2. Values used for the booster converter.

Component	Value
Inductor (L)	100 µH
Capacitor (C_{PV})	680 µH
Resistor (R_{eq})	0.1986 Ω
(V_{DC}) Voltage	30 V
PWM_{boost}	100 kHz
Voltage and current sampling time	20 µs

IoT

As outlined in the preceding section, the IoT infrastructure is implemented on the ARM Cortex M3 processor. This processor features two critical peripherals that enable IoT functionality: the Ethernet peripheral and the Inter-Processor Communication peripheral, which facilitates data transfer between the M3 and the real-time control processor (DSP). Implementing the OSI (Open Systems Interconnection) model via software is requisite. The external hardware and the ARM processor handle the physical and network access layers. The remaining layers are software-defined. In the Internet layer, IP addresses identify the source and destination hosts. The Transport layer uses TCP, while the Application layer relies on HTTP alongside custom application commands, as detailed in **Table 3.**

© 2024 The Author(s). | Published by Institute of Smart Energy Systems Press

Table 3. Custom application commands.

Command	Description
C2	Initiates the PV panel emulator.
C3	Terminates the PV panel emulator.
C4	Retrieves the instantaneous PV output power.
C5	Retrieves the calculated theoretical PV power.
C6	Performs a single acquisition of v_{PV}.
C7	Performs a single acquisition of i_L.
C8	Performs a single acquisition of V_{DC}.
C9	Obtains the irradiance measurement value.
CA	Modifies the SMC/SMPIC controller parameters.
CB	Begins data acquisition for i_{Lref}, and i_L, or v_{PV}, and v_{PVref}.
CC	Accesses the first acquisition buffer specified by command 0xCB.
CD	Accesses the second acquisition buffer specified by command 0xCB.

GA

The primary goal of the GA is to discover the most effective parameters for both SMC and SMPIC. For SMC, these parameters correspond to **Eqs. 8 and 9** for the inner current loop, and **Eqs. 10 and 11** for the outer voltage loop. For SMPIC, the parameters are associated with **Eq. 6** for the current loop and **Eq. 5** for the voltage loop, in addition to the parameters from (6) applicable to both loops. In prior research, SMC parameters were derived through mathematical modeling [11], whereas SMPIC parameters were determined using a heuristic PSO algorithm in simulation before being applied to the physical prototype [10]. However, the physical boost converter exhibits certain practical characteristics—such as component tolerances, temperature variations, rounding errors, and operational constraints—that were omitted in simulations. By executing directly on the physical prototype, the GA ensures the identification of genuinely optimal results.

The GA is implemented using MATLAB, following the methodology described before. Specific constraints are established: the maximum number of iterations is capped at 100; the population size is fixed at 10; and the fitness function targets a settling time of 20 ms and 1 ms for voltage and current, respectively, along with a maximum overshoot limit of 10% during step testing.

Operating on a cloud server, the GA generates an initial random population (representing parameter sets), which is transmitted over the network **(Table 3)** and integrated into the SMC or SMPIC of the physical boost converter prototype. The DSP captures voltage and current data and transmits it back to the server every 1 s. The GA then evaluates the signal quality against the predefined fitness function constraints (Plant evaluation), as illustrated in **Figure 2**. Multiple iterations are required to converge on the optimal solution.

This experimental configuration presents several drawbacks: discovering the optimal values requires more time compared to simulation-based methods; unfavorable chromosomes (inherent to the GA process) may introduce transient spikes during plant evaluation; the time-intensive nature of the GA limits both iteration count and population size; and the

© 2024 The Author(s). | Published by Institute of Smart Energy Systems Press

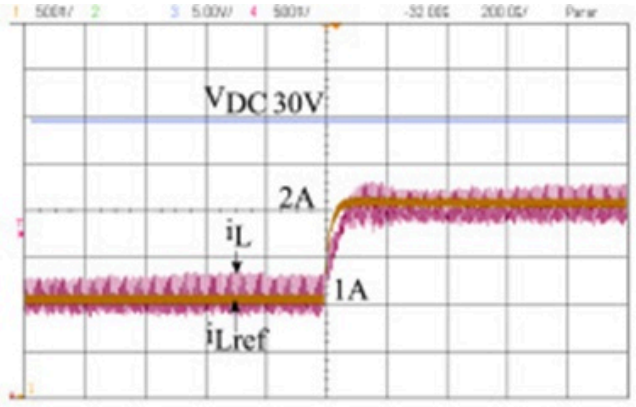
processor must possess sufficient computational power to handle simultaneous control tasks and TCP/IP communications. Consequently, the system operates in two distinct modes: normal mode and optimization mode.

Normal mode represents standard PV system operation, dedicated to monitoring power, voltage, and current, while continuously executing the MPPT algorithm and control loops. During this phase, parameters remain locked to prevent performance degradation or unwanted transients.

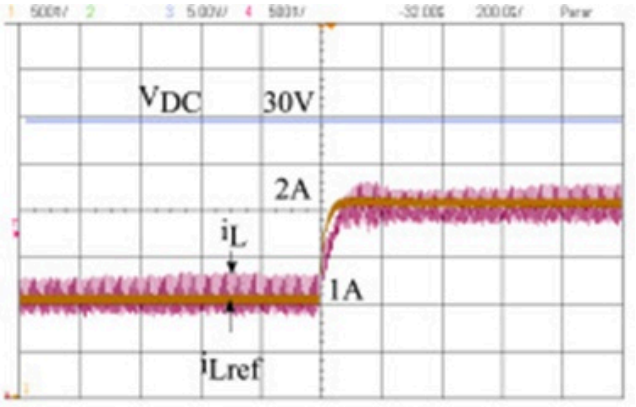
In optimization mode, the software facilitates data exchange between the server and the hardware, allowing for the reconfiguration of SMPIC or SMC via custom commands. Because the optimization routine is inherently slow in identifying peak performance, any interruption in the communication link will trigger a fallback, returning the system to normal mode using the most recent optimal parameters.

The purpose of this initial experiment is to establish the optimal parameters for the current control loop. Following the execution of the GA in optimization mode, the inductor current was measured under normal mode conditions. As illustrated in **Figure 4**, the current successfully tracked its reference both before and after the SMPIC parameter calibration when a reference step from 1.0 to 2.0 A was applied to evaluate the response. This performance is more clearly depicted in **Figure 4c**, which presents network-acquired data comparing the w-PSO and GA SMPIC parameters. An identical testing procedure is shown in **Figure 5**, demonstrating the system before and after GA calibration, while **Figure 5c** displays network data comparing heuristic and deterministic SMC parameters. Across all scenarios, the outcomes are comparable, as summarized in **Table 4**. Consequently, the GA tuning demonstrates highly satisfactory performance in terms of settling time and steady-state parameters.

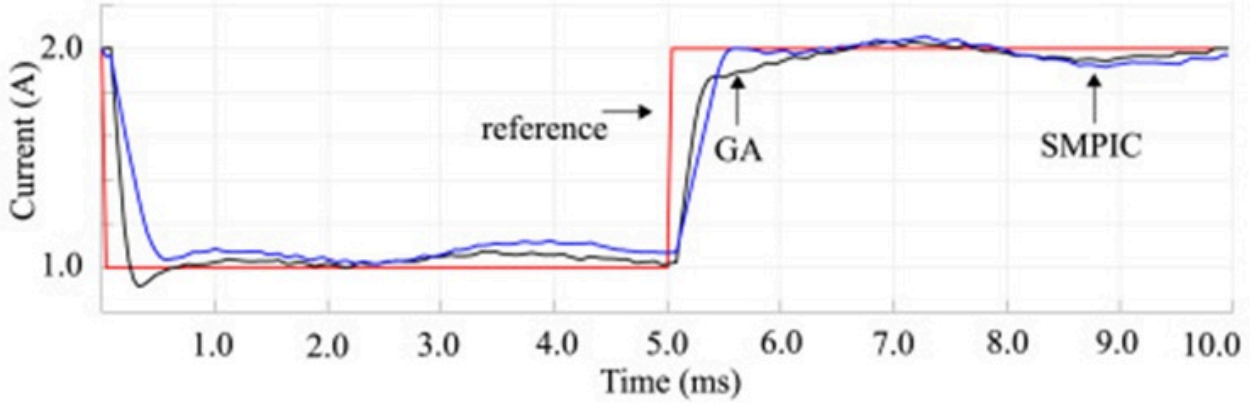
© 2024 The Author(s). | Published by Institute of Smart Energy Systems Press



(a) w-PSO current loop SMPIC in detail measured on solar explorer kit prototype.



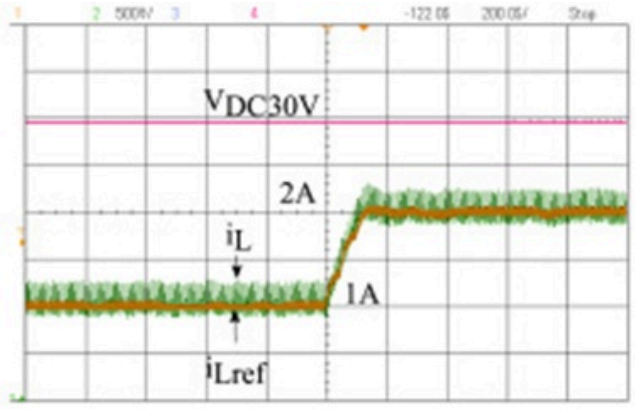
(b) GA adjusted current loop SMPIC measured on solar explorer kit prototype.



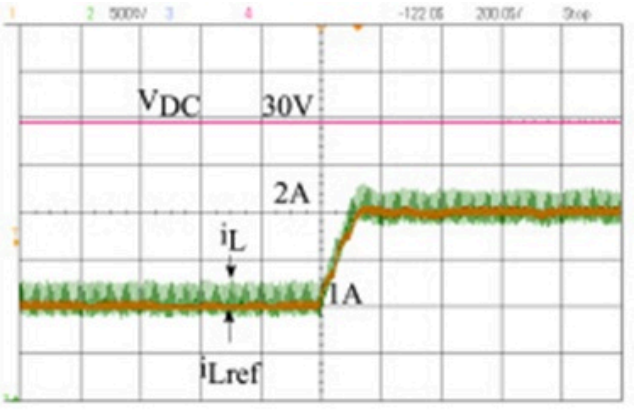
(c) Current loop comparison acquired through network on solar explorer kit prototype: (SMPIC) w-PSO SMPIC; (GA) Heuristic SMPIC.

Figure 4. Current loop measured on bench.

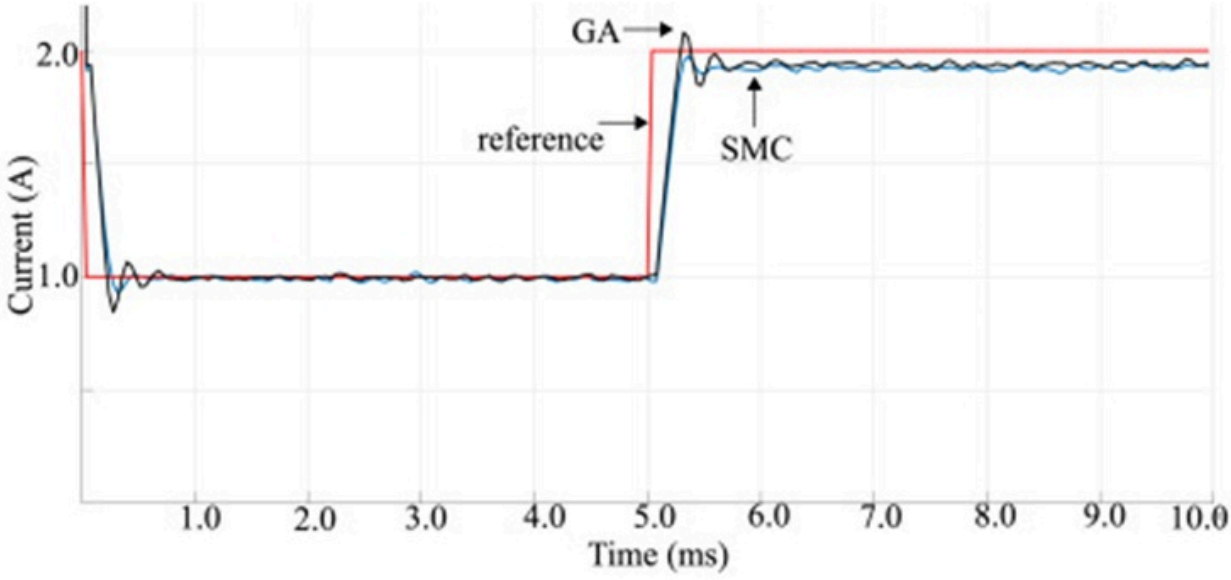
© 2024 The Author(s). | Published by Institute of Smart Energy Systems Press



(a) Deterministic current control loop SMC measured on solar explorer kit prototype.

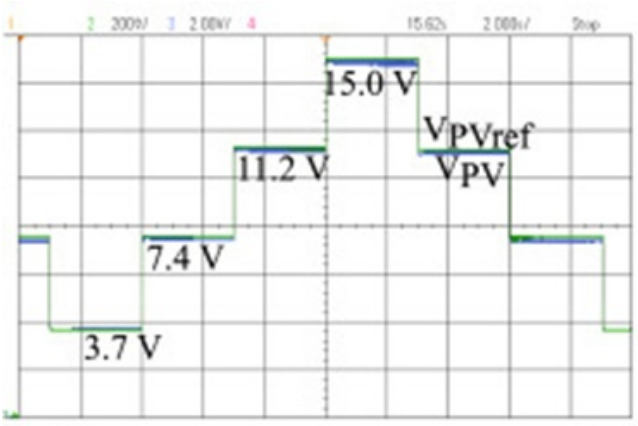


(b) GA adjusted current loop SMC measured on solar explorer kit prototype.

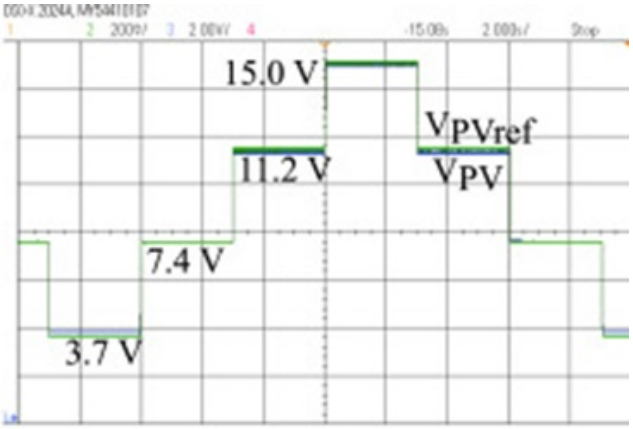


(c) Current control loop comparison acquired through network on solar explorer kit prototype: (SMC) Deterministic SMC; (GA) Heuristic SMC.

Figure 5. Current control loop measured on bench.



(a) GA voltage control loop SMPIC.

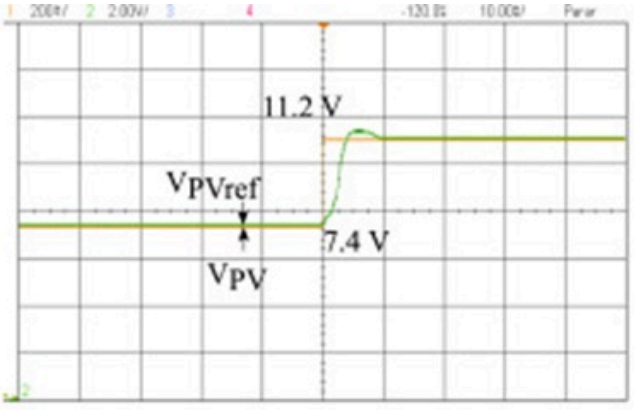


(b) GA voltage control loop SMC.

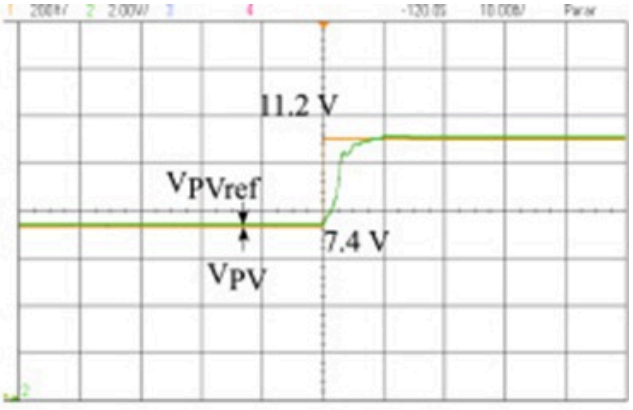
© 2024 The Author(s). | Published by Institute of Smart Energy Systems Press

Figure 6. Voltage control loop measured on bench.

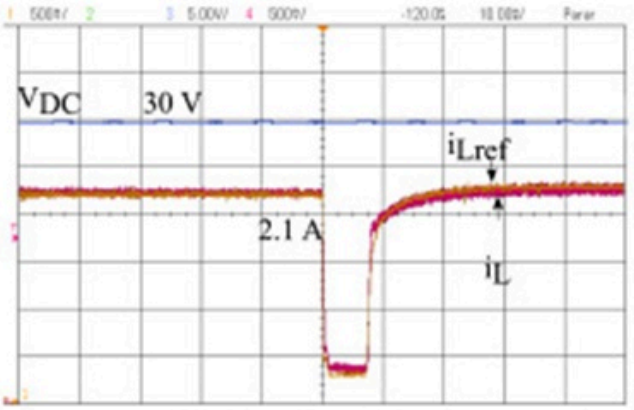
© 2024 The Author(s). | Published by Institute of Smart Energy Systems Press



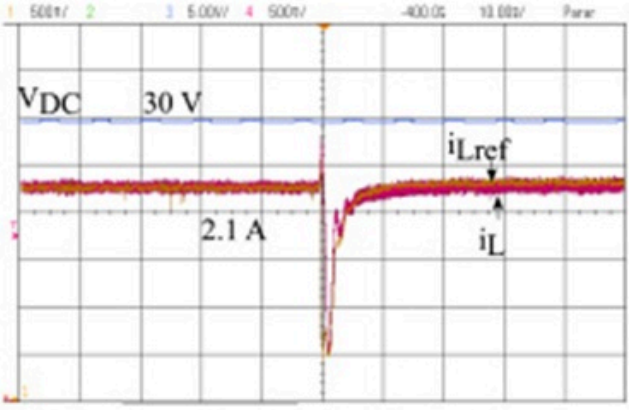
(a) GA adjusted voltage loop SMPIC step response.



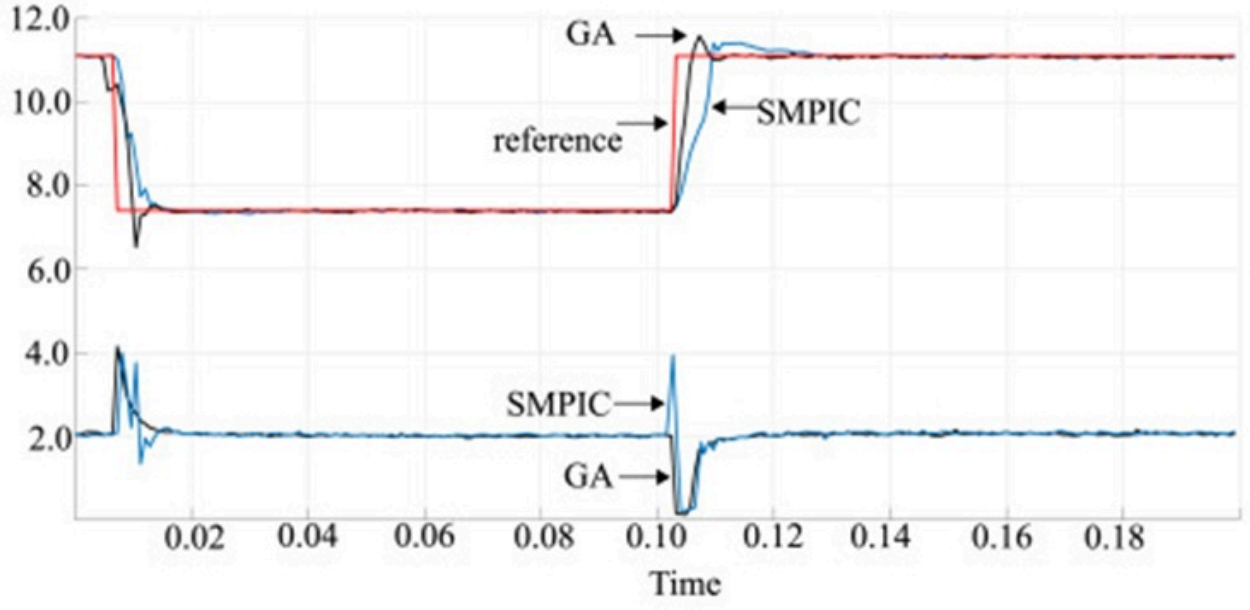
(b) Voltage loop SMPIC step response.



(c) Current behavior for GA adjusted voltage loop step.



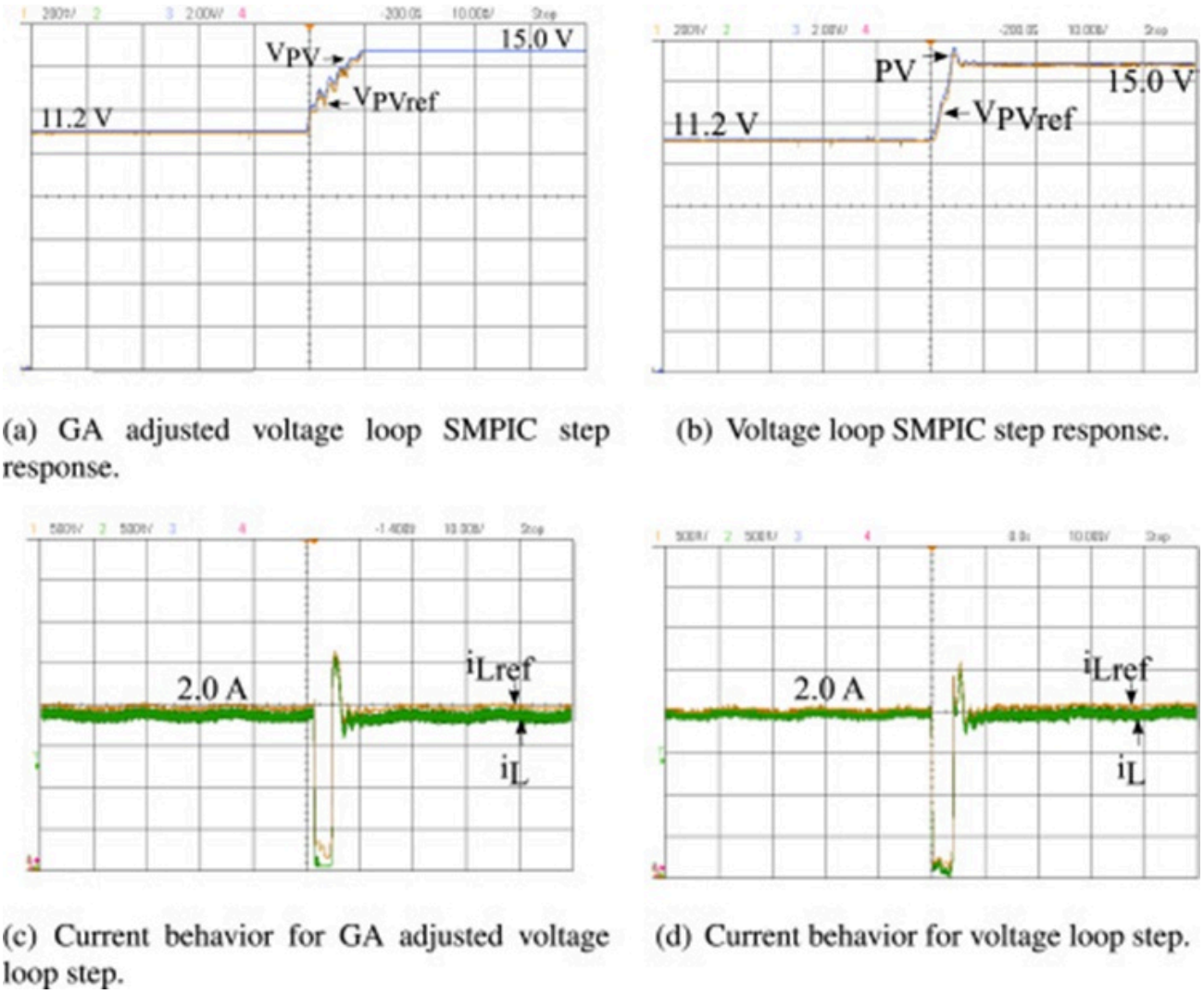
(d) Current behavior for voltage loop step.



(e) Voltage loop compare and current acquired through network on solar explorer kit prototype: (SMPIC) Deterministic SMPIC; (GA) Heuristic SMPIC.

© 2024 The Author(s). | Published by Institute of Smart Energy Systems Press

Figure 7. Voltage loop step test measured on solar explorer kit prototype—irradiance from 400 W/m2 to 600 W/m2.



(a) GA adjusted voltage loop SMPIC step response.

(b) Voltage loop SMPIC step response.

(c) Current behavior for GA adjusted voltage loop step.

(d) Current behavior for voltage loop step.

Figure 8. Voltage loop step test measured on solar explorer kit prototype—irradiance from 600 W/m2 to 800 W/m2.

Current control loop performance comparison

The purpose of this initial experiment is to establish the optimal parameters for the current control loop. Following the execution of the GA in optimization mode, the inductor current was measured under normal mode conditions. As illustrated in **Figure 4**, **Figure 4,** the current successfully tracked its reference both before and after the SMPIC parameter calibration when a reference step from 1.0 to 2.0 A was applied to evaluate the response. This performance is more clearly depicted in **Figure 4c**, which presents network-acquired data comparing the w-PSO and GA SMPIC parameters. An identical testing procedure is shown in **Figure 5**, **Figure 5**, demonstrating the system before and after GA calibration, while **Figure 5c** displays network data comparing heuristic and deterministic SMC parameters. Across all scenarios, the outcomes are comparable, as summarized in **Table 4**. Consequently, the GA tuning demonstrates highly satisfactory performance in terms of settling time and steady-state parameters.

Table 4. Current step test comparison.

© 2024 The Author(s). | Published by Institute of Smart Energy Systems Press

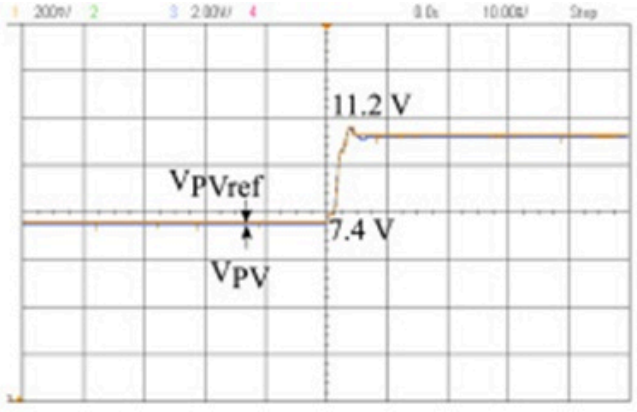
	SMPIC		SMC	
	w-PSO	**GA**	**Deterministic**	**GA**
Settling time	1 ms	1 ms	0.41 ms	0.4 ms
Overshoot	0%	0%	0%	1.1%
Steady-state error	5.1%	2.6%	2.5%	2.4%

Performance voltage control loop comparison

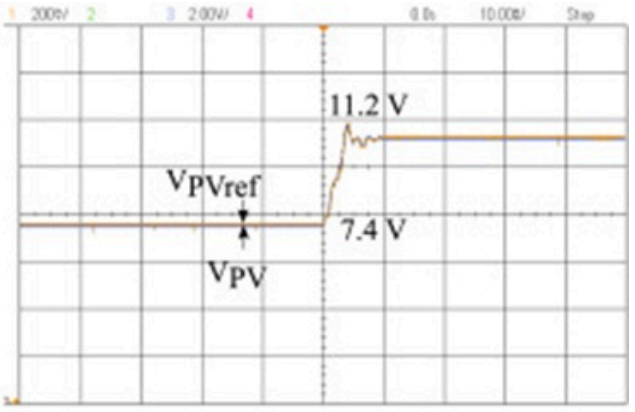
After evaluating the inner control loop, the subsequent phase involves using the GA to assess the parameters of the outer voltage control loop, which inherently encompasses the inner current control loop. **Figure 6** illustrates tests across four distinct voltage reference levels (3.7 V, 7.4 V, 11.2 V and 15.0 V), all of which achieved zero steady-state error.

Bench measurements for a voltage step utilizing SMPIC are illustrated in **Figure 7** during an irradiance shift from 400 W/m2 to 600 W/m2, and in **Figure 8** during an irradiance shift from 600 W/m2 to 800 W/m2, detailing the system before and after parameter adjustment. Similarly, for the SMC, parallel tests are shown in **Figures 9a-9d** and **Figures 10a-10d.** These results are more clearly detailed in **Figures 7 and 9**, where the step voltage reference transitions between two levels: 7.4 V to 11.2 V, and subsequently from 11.2 V to 15.0 V. It is evident that the proposed optimization technique outperforms both the w-PSO SMPIC and the deterministic SMC, exhibiting superior settling times and reduced overshoot, as documented in **Table 5**. Furthermore, the current response during both tests maintains minimal overshoot when GA optimization is applied.

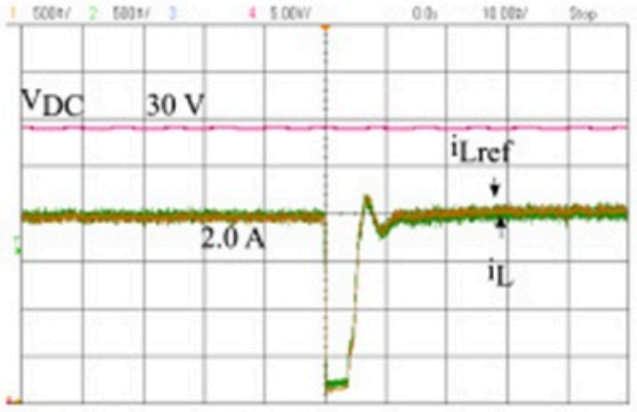
© 2024 The Author(s). | Published by Institute of Smart Energy Systems Press



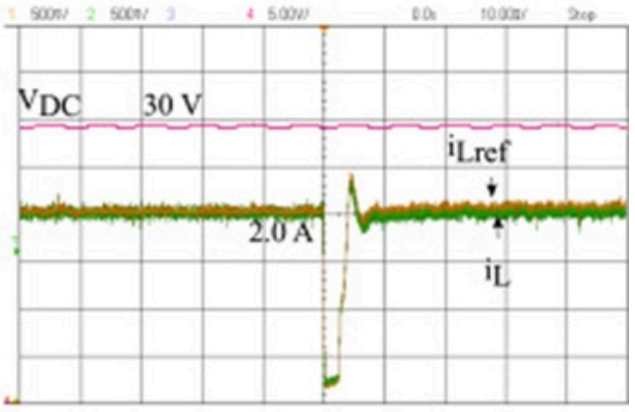
(a) GA adjusted voltage loop SMC step response.



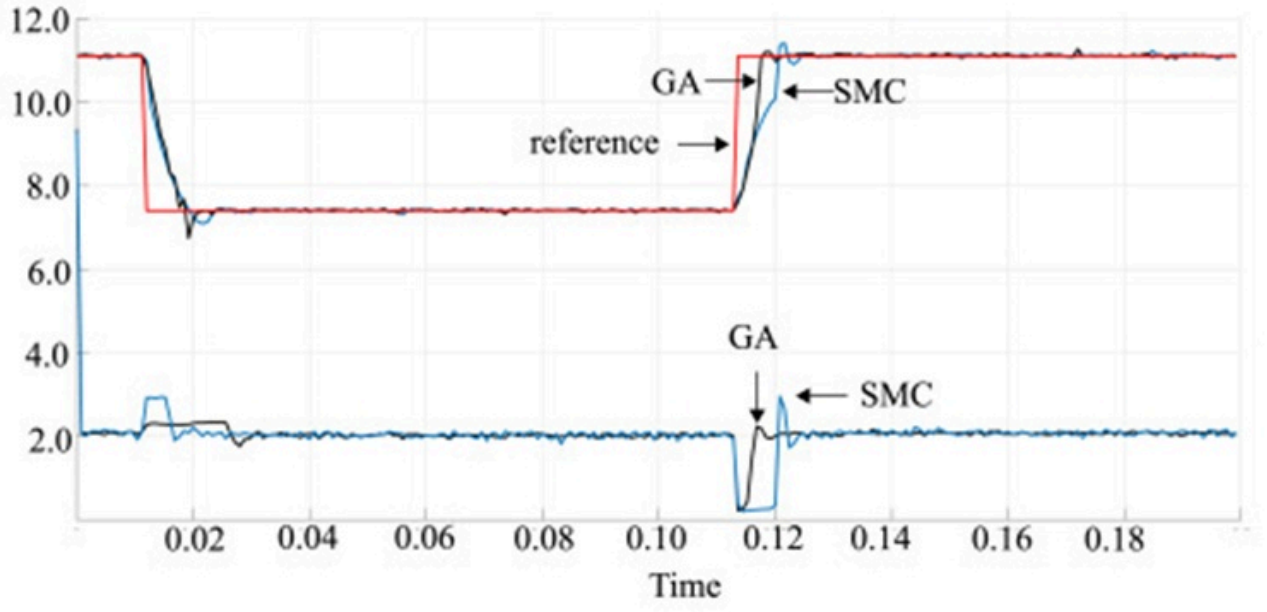
(b) Voltage loop SMC step response.



(c) Current behavior for GA adjusted voltage loop step.



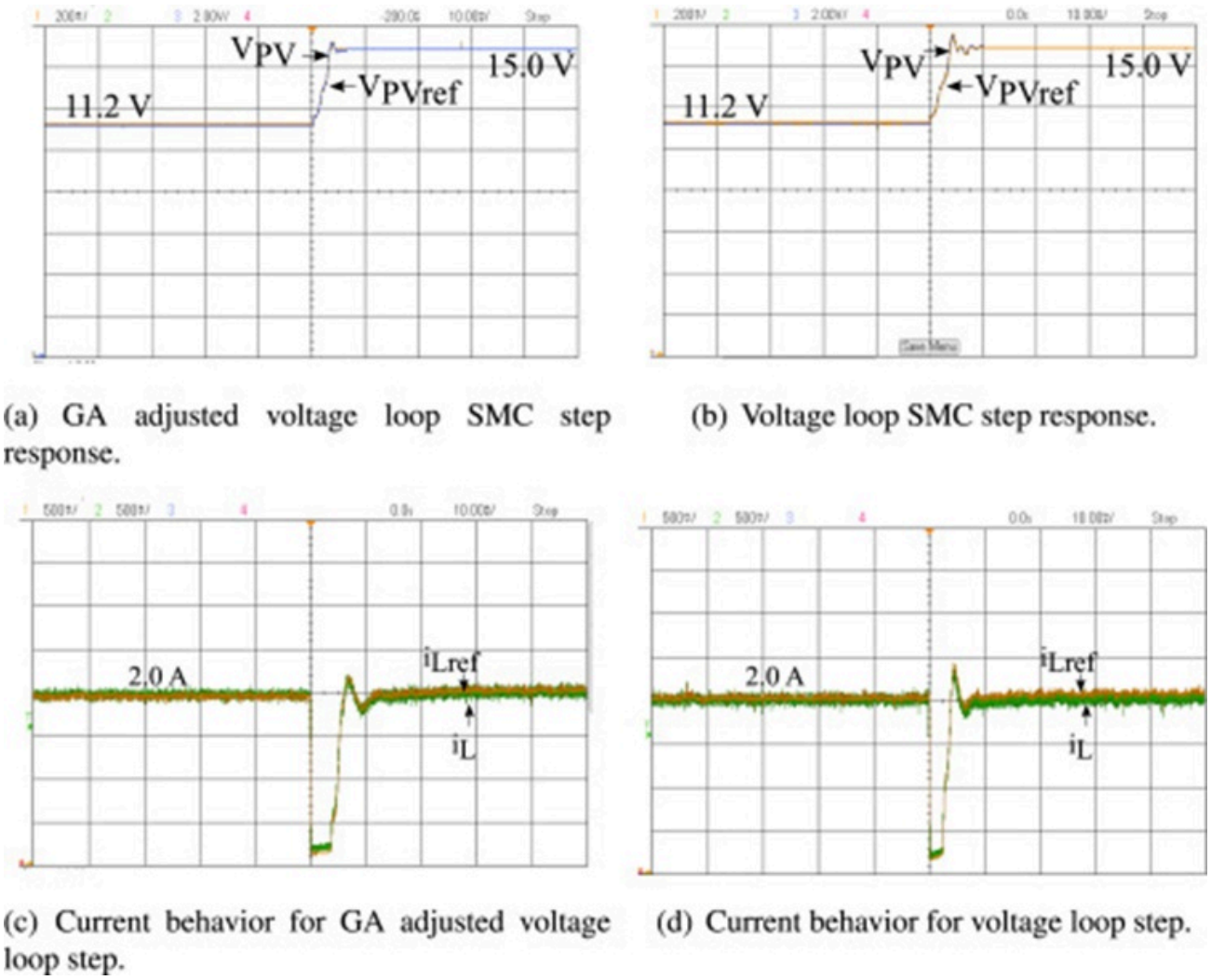
(d) Current behavior for voltage loop step.



(e) Voltage loop compare and current acquired through network on solar explorer kit prototype: (SMC) Deterministic SMC; (GA) Heuristic SMC.

© 2024 The Author(s). | Published by Institute of Smart Energy Systems Press

Figure 9. Voltage loop step test measured on solar explorer kit prototype—irradiance from 400 W/m2 to 600 W/m2.



(a) GA adjusted voltage loop SMC step response.

(b) Voltage loop SMC step response.

(c) Current behavior for GA adjusted voltage loop step.

(d) Current behavior for voltage loop step.

Figure 10. Voltage loop step test measured on solar explorer kit prototype—irradiance from 600 W/m2 to 800 W/m2.

Table 5. Voltage step test comparison.

Voltage		SMPIC		SMC	
		w-PSO	GA	Deterministic	GA
	Settling time	16 ms	9 ms	10 ms	7 ms
7.4 to 11.2 V	**Overshoot**	4.6%	5.4%	1.8%	0.9%
	Steady-state error	0%	0%	0%	0%
	Settling time	9 ms	9 ms	10 ms	6 ms
11.2 to 15.0 V	**Overshoot**	2.7%	0.1%	2.7%	1.3%
	Steady-state error	0%	0%	0%	0%

© 2024 The Author(s). | Published by Institute of Smart Energy Systems Press

MPPT algorithm

Following the validation of the control loops, the subsequent evaluation examines the performance of the newly derived SMC and SMPIC parameters under a stepped irradiation profile. **Figures 11 and 12** illustrate the PV control system's behavior during irradiance fluctuations. The system was tested across irradiance levels ranging from 200 to 800 W/m2, confirming the controller's reliability under standard operating scenarios. The data observed in **Figures 11 and 12** align consistently with the parameters detailed in **Table 1**. During this evaluation, the incremental conductance MPPT method is utilized to determine the voltage reference [36]. The results indicate that vPV successfully tracks vPVref, while the inductor current iL similarly follows its reference iLref, all while the boost converter's output voltage is sustained at approximately 30 V.

Conversely, **Figures 13 and 14**, corresponding to SMC and SMPI, respectively, depict an irradiance shift from 200 up to 800 W/m2 and rapidly back down to 200 W/m2, demonstrating exceptional stability. During each irradiance step, a minor fluctuation is introduced to simulate rapid PV shading; throughout this process, VPV consistently tracks VPVref.

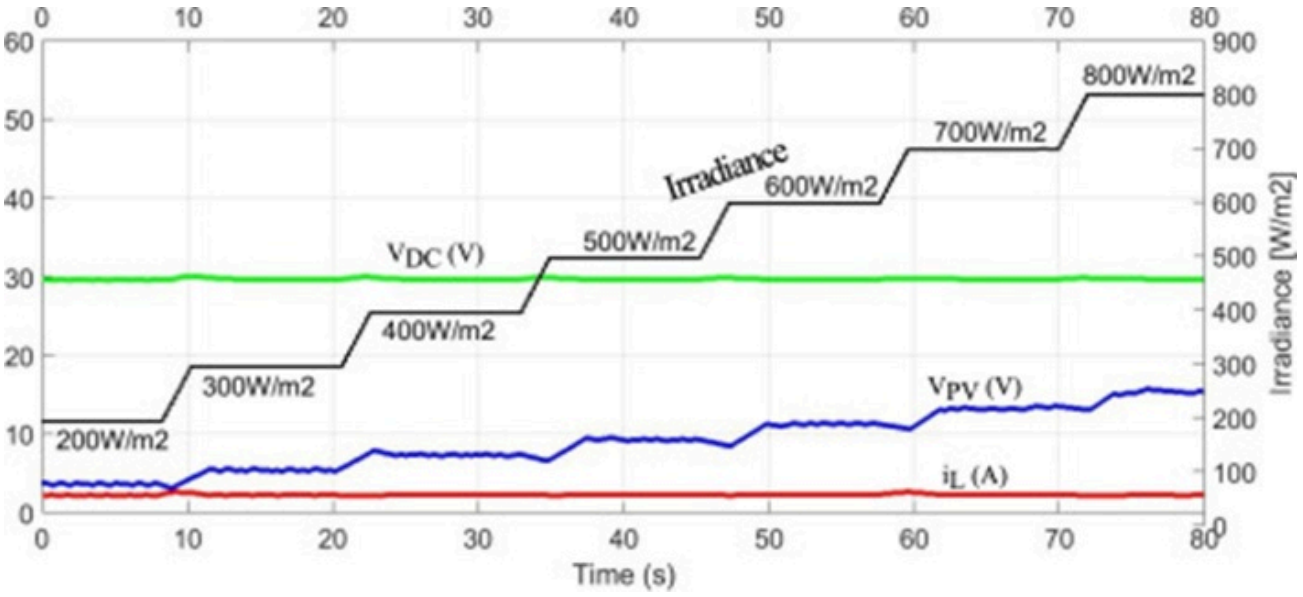
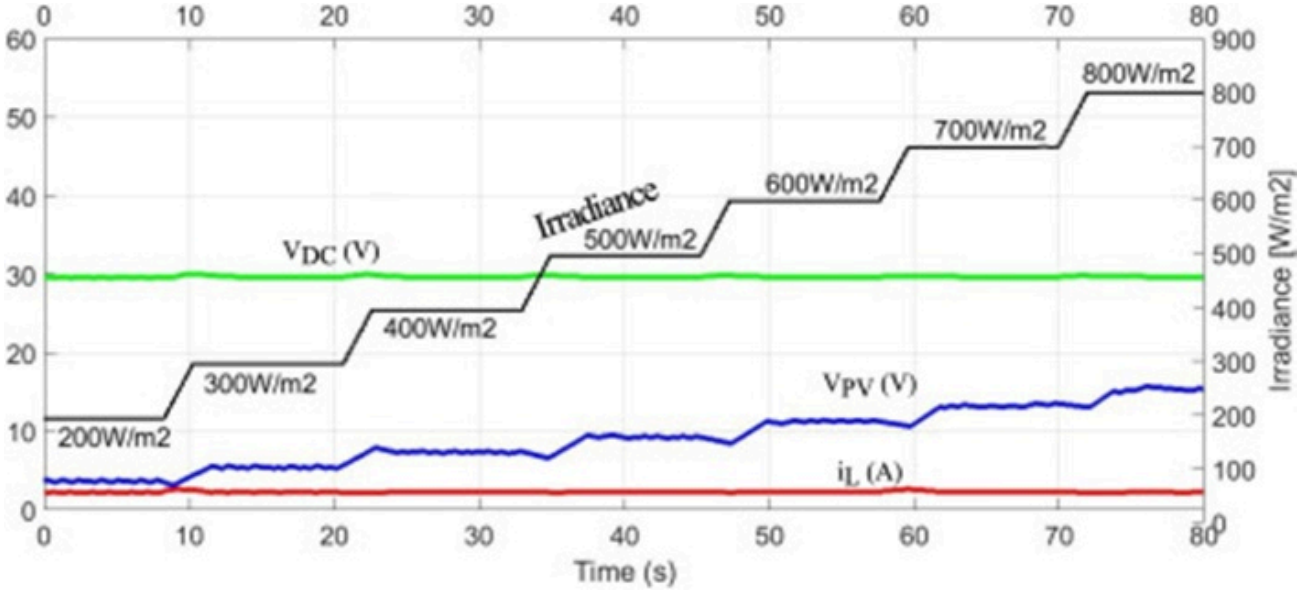


Figure 11. Irradiation variation test for SMC.



© 2024 The Author(s). | Published by Institute of Smart Energy Systems Press

Figure 12. Irradiation variation test for SMPIC.

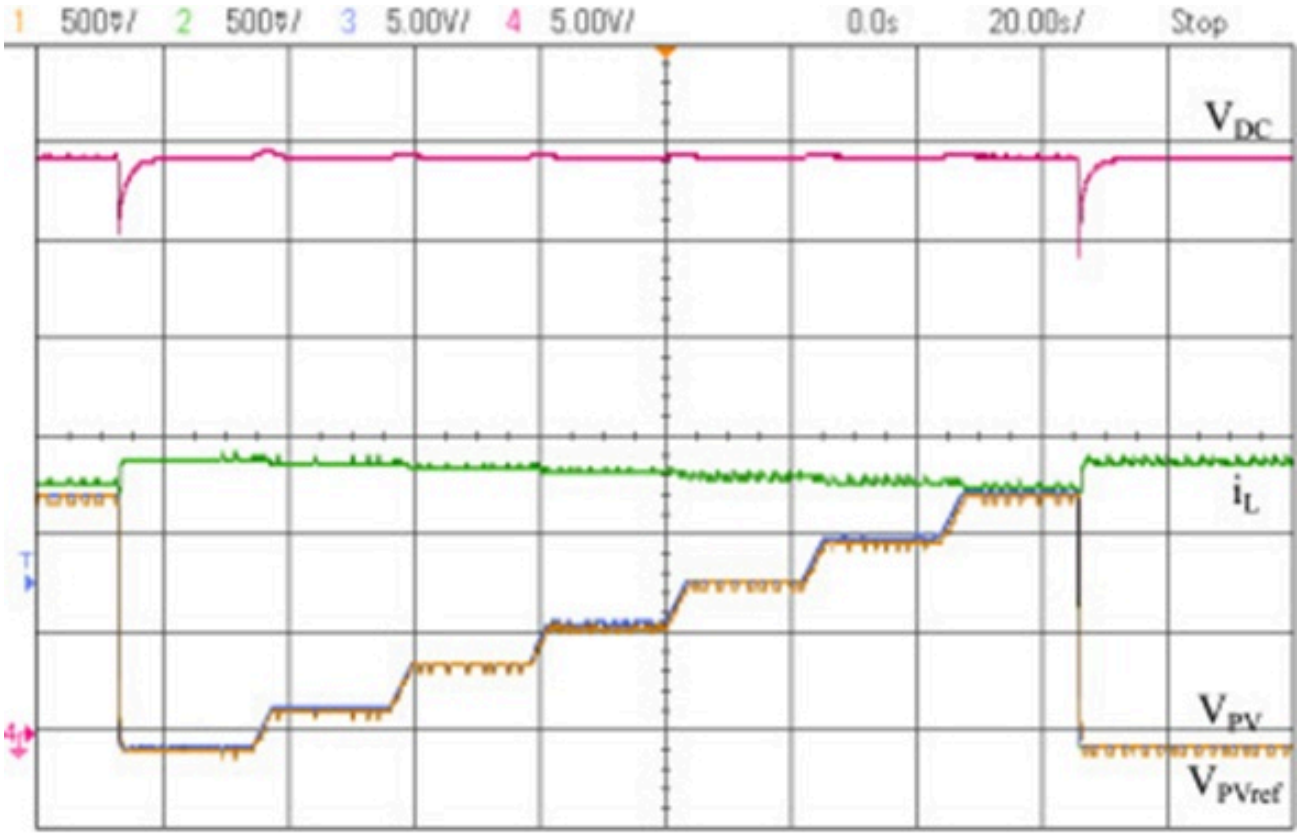


Figure 13. Irradiance—fast variance under SMC control.

© 2024 The Author(s). | Published by Institute of Smart Energy Systems Press

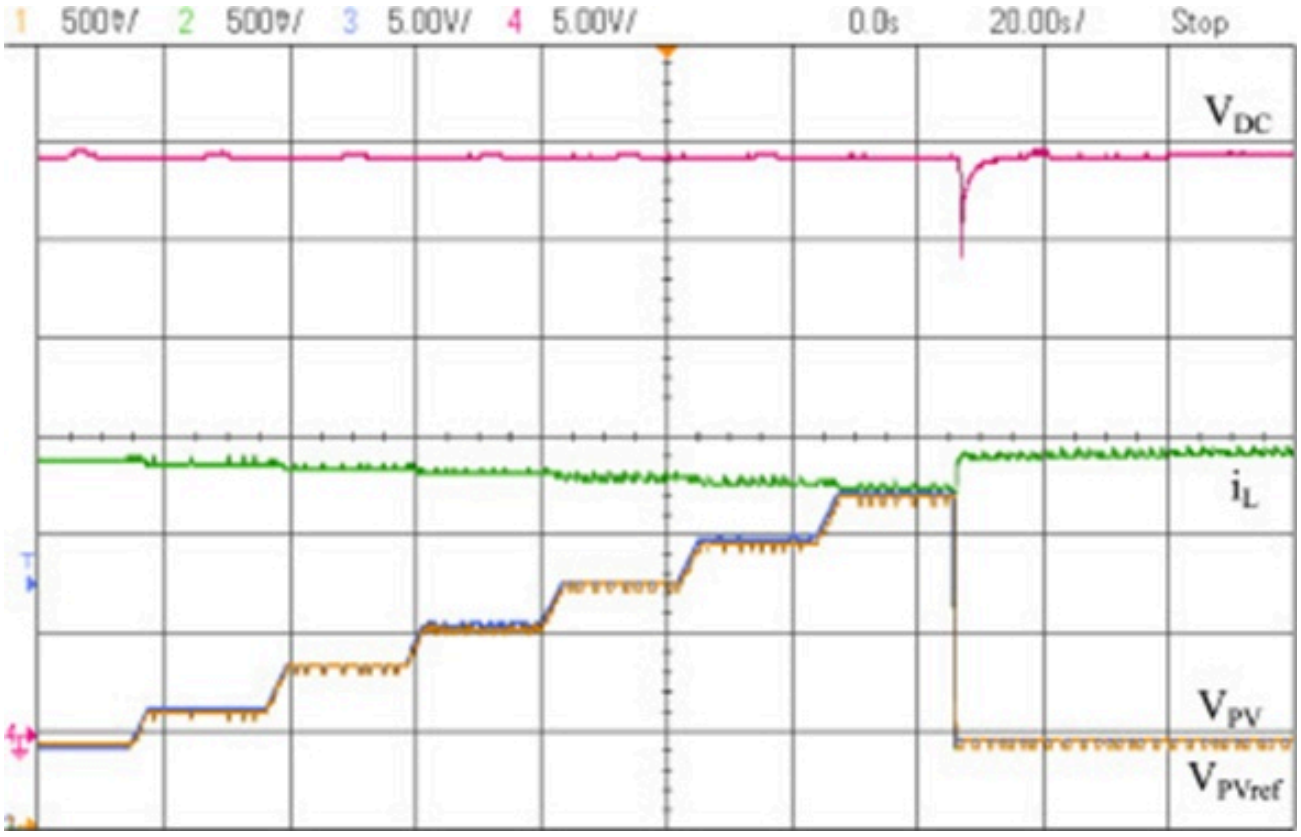


Figure 14. Irradiance—fast variance under SMPI control.

Conclusion

This manuscript extends previous research [10, 11], which introduced SMPIC and SMC frameworks for a PV system's boost converter operating at a constant switching frequency. In those preceding studies, empirical tests contrasted the performances of SMC and SMPIC against a lead-lag controller, with the proposed methods demonstrating superior results. Consequently, further elaboration on the comparative superiority of these two controllers is omitted here.

Typically, most research executes the GA within a simulation environment, such as MATLAB, before deploying the derived parameters to physical hardware. This conventional approach suffers from inherent drawbacks, including component tolerances and temperature-induced variations. Furthermore, the mathematical modeling of SMC or SMPIC requires assumptions, constraints, approximations, and linearizations that can degrade real-world performance. The primary innovation of this study is enhancing SMPIC and SMC performance by executing the GA directly on a physical converter prototype within an IoT ecosystem, thereby mitigating the aforementioned simulation-based limitations. The physical plant communicates with a cloud server via TCP/IP. The server hosts the GA algorithm, facilitating the tuning of the SMC gains. Because the optimization sequence is relatively slow and may induce temporary spikes, the system transitions to normal operating mode once the optimal parameters are identified. Optimization mode can be reactivated on demand whenever necessary.

This research demonstrates that the dynamically tuned controllers outperform previously established SMPIC and SMC boost converters across both voltage and current control loops, evidenced by improvements in voltage step overshoot and settling times. While earlier methodologies relied on simulated w-PSO to optimize parameters before hardware implementation, the versatile technique proposed herein yields superior outcomes by enabling runtime optimization. Even

© 2024 The Author(s). | Published by Institute of Smart Energy Systems Press

under varying irradiation conditions, the controllers exhibit highly satisfactory performance, characterized by rapid response times, minimal steady-state error, and enhanced output stability.

The realization of this architecture is facilitated by the DSP's dual capability to execute real-time control algorithms and manage internet communications simultaneously. Ultimately, the integration of IoT concepts introduces robust new capabilities for system calibration, diagnostics, and continuous monitoring.

Acknowledgements

CNPq - Conselho Nacional de Desenvolvimento Científico e Tecnológico grant ID: 407867/2022-8 and FAPESP - Fundação de Amparo à Pesquisa do Estado de São Paulo grant ID: 2022/00323-3.

Conflict of interest

None

Financial support

None

Ethics statement

None

Received: 11 May 2023 Revised: 17 Jul 2023 Accepted: 03 Aug 2023
Published online: 15 November 2024

Rights and permissions

Open Access The author(s) retain copyright. This article is licensed under the Creative Commons Attribution-NonCommercial-ShareAlike 4.0 International License. It may be shared and adapted for non-commercial purposes with appropriate attribution, an indication of changes, and distribution of adaptations under the same license. Third-party material may be subject to separate terms identified in its credit line. View the license at https://creativecommons.org/licenses/by-nc-sa/4.0/.

References

1. Karami N, Moubayed N, Outbib R. General review and classification of different MPPT techniques. Renew Sustain Energy Rev. 2017;68:1-8. https://doi.org/10.1016/j.rser.2016.09.132.

2. Mirzal A, Yoshii S, Furukawa M. PID parameters optimization by using genetic algorithm: A study on time-delay systems. ISTECS J. 2006;8:34-43.

3. Fernandes D, Almeida R, Guedes T, Sguarezi Filho A, Costa F. State feedback control for DC-photovoltaic systems. Electr Power Syst Res. 2017;143:794-801. https://doi.org/10.1016/j.epsr.2016.08.037.

4. Ilyas A, Khan MR, Ayyub M. FPGA based real-time implementation of fuzzy logic controller for maximum power point tracking of solar photovoltaic system. Optik. 2020;213:164668. https://doi.org/10.1016/j.ijleo.2020.164668.

5. Njomo AFT, Sonfack LL, Douanla RM, Kenne G. Nonlinear neuro-adaptive control for MPPT applied to photovoltaic systems. J Control Autom Electr Syst. 2021;32(3):693-702. https://doi.org/10.1007/s40313-021-00691-3.

6. Bellinaso LV, Figueira HH, Basquera MF, Vieira RP, Gründling HA, Michels L. Cascade control with adaptive voltage controller applied to photovoltaic boost converters. IEEE Trans Ind Appl. 2019;55(2):1903-12. https://doi.org/10.1109/TIA.2018.2884904.

7. Cunha R, Inomoto R, Altuna J, Costa F, Di Santo S, Sguarezi Filho A. Constant switching frequency finite control set model predictive control applied to the boost converter of a photovoltaic system. Sol Energy. 2019;189:57-66. https://doi.org/10.1016/j.solener.2019.07.021.

8. Filho AJS, Inomoto RS, Rodrigues LL, Cunha RBA, Vilcanqui OAC. Predictive control applied to a boost converter of a photovoltaic system. J Control Autom Electr Syst. 2021. https://doi.org/10.1007/s40313-021-00796-9.

9. Priyadarshi N, Padmanaban S, Bhaskar Ranjana M, Azam F, Taha I, Mousa Hussien MG, et al. An adaptive TS-fuzzy model based RBF neural network learning for grid integrated photovoltaic applications. Renew Power Gener IET. 2022;16. https://doi.org/10.1049/rpg2.12505.

10. Vargas Gil GM, Lima Rodrigues L, Inomoto RS, Sguarezi AJ, Machado Monaro R. Weighted-PSO applied to tune sliding mode plus PI controller applied to a boost converter in a PV system. Energies. 2019;12(5). https://doi.org/10.3390/en12050864.

11. Inomoto RS, Monteiro JRBA, Sguarezi Filho AJ. Boost converter control of PV system using sliding mode control with integrative sliding surface. IEEE J Emerg Sel Top Power Electron. 2022;1-1. https://doi.org/10.1109/JESTPE.2022.3158247.

12. Bounar N, Labdai S, Boulkroune A. PSO–GSA based fuzzy sliding mode controller for DFIG-based wind turbine. ISA Trans. 2019;85:177-88. https://doi.org/10.1016/j.isatra.2018.10.020.

13. Holland JH. Adaptation in natural and artificial systems: an introductory analysis with applications to biology, control, and artificial intelligence. MIT Press; 1992.

14. Benhlima S, Chaymaa L, Bekri A. Genetic algorithm based approach for autonomous mobile robot path planning. Procedia Comput Sci. 2018;127. https://doi.org/10.1016/j.procs.2018.01.113.

15. Wang Q, Xi H, Deng F, Cheng M, Buja G. Design and analysis of genetic algorithm and BP neural network based PID control for boost converter applied in renewable power generations. IET Renew Power Gener. 2022;16(7):1336-44. https://doi.org/10.1049/rpg2.12320.

16. Sivamani D, Shyam D, Ali AN, Premkumar K, Narendiran S, Alexander SA. Solar powered battery charging system using optimized PI controller for buck boost converter. IOP Conf Ser: Mater Sci Eng. 2021;1055(1):012151.

17. Silverio M, Renukappa S, Suresh S. What is a smart device? - A conceptualisation within the paradigm of the internet of things. Vis Eng. 2018;6. https://doi.org/10.1186/s40327-018-0063-8.

© 2024 The Author(s). | Published by Institute of Smart Energy Systems Press

18. Potter C, Hancke G, Silva B. Machine-to-machine: Possible applications in industrial networks. In: 2013 IEEE International Conference on Industrial Technology (ICIT). 2013. p. 1321-6. https://doi.org/10.1109/ICIT.2013.6505864.

19. Rouibah N, Barazane L, Benghanem M, Mellit A. IoT-based low-cost prototype for online monitoring of maximum output power of domestic photovoltaic systems. ETRI J. 2021;43(3):459-70. https://doi.org/10.4218/etrij.2019-0537.

20. J B, Moses M. IOT based augmented perturb-and-observe soft switching boost converters for photovoltaic power systems in smart cities. Wirel Pers Commun. 2018;102:2619-41. https://doi.org/10.1007/s11277-018-5280-x.

21. Rouibah N, Barazane L, Mellit A, Hajji B, Rabhi A. A low-cost monitoring system for maximum power point of a photovoltaic system using IoT technique. In: 2019 International Conference on Wireless Technologies, Embedded and Intelligent Systems (WITS). 2019. p. 1-5. https://doi.org/10.1109/WITS.2019.8723724.

22. Rokonuzzaman M, Shakeri M, Hamid FA, Mishu MK, Pasupuleti J, Rahman KS, et al. IoT-enabled high efficiency smart solar charge controller with maximum power point tracking—Design, hardware implementation and performance testing. Electronics. 2020;9(8). https://doi.org/10.3390/electronics9081267.

23. Habib M, Gram A, Harrag A, Wang Q. Optimized management of reactive power reserves of transmission grid-connected photovoltaic plants driven by an IoT solution. Int J Electr Power Energy Syst. 2022;143:108455. https://doi.org/10.1016/j.ijepes.2022.108455.

24. Erickson RW, Maksimovic D. Fundamentals of power electronics. Kluwer Academic Publishers; 2004.

25. Mohan N, Undeland TM, Robbins WP. Power electronics - converters, applications, and design. John & Sons, Inc; 1995.

26. Villalva M, de Siqueira T, Ruppert E. Voltage regulation of photovoltaic arrays: small-signal analysis and control design. IET Power Electron. 2010;3:869-80. https://doi.org/10.1049/iet-pel.2008.0344.

27. Rezaei MM, Asadi H. A modified perturb-and-observe-based maximum power point tracking technique for photovoltaic energy conversion systems. J Control Autom Electr Syst. 2019;30. https://doi.org/10.1007/s40313-019-00495-6.

28. Trindade FS, Filho AJS, Jacomini RV, Ruppert E. Experimental results of sliding-mode power control for doubly-fed induction generator. In: 2013 Brazilian Power Electronics Conference. 2013. p. 686-91. https://doi.org/10.1109/COBEP.2013.6785189.

29. Monteiro JRBA, Oliveira CMR, Almeida TEP, Cezare MJ. Pseudo sliding mode control with integrative action applied to brushless DC motor speed control. In: 2015 IEEE 13th Brazilian Power Electronics Conference and 1st Southern Power Electronics Conference (COBEP/SPEC). 2015. p. 1-6. https://doi.org/10.1109/COBEP.2015.7420076.

30. Aghaei M, Esksndari A, Reinders A. Autonomous monitoring and analysis of PV systems by unmanned aerial vehicles, internet of things and big data analytics. In: Conference: 37th European Photovoltaic Solar Energy Conference and Exhibition. 2020. https://doi.org/10.4229/EUPVSEC20202020-5DO.3.5.

31. Shukla A, Pandey HM, Mehrotra D. Comparative review of selection techniques in genetic algorithm. In: 2015 International Conference on Futuristic Trends on Computational Analysis and Knowledge Management (ABLAZE). 2015. p. 515-9. https://doi.org/10.1109/ABLAZE.2015.7154916.

© 2024 The Author(s). | Published by Institute of Smart Energy Systems Press

32. Zhong J, Hu X, Zhang J, Gu M. Comparison of performance between different selection strategies on simple genetic algorithms. In: International Conference on Computational Intelligence for Modelling, Control and Automation and International Conference on Intelligent Agents, Web Technologies and Internet Commerce (CIMCA-iAWTIC'06). Vol. 2. 2005. p. 1115-21. https://doi.org/10.1109/CIMCA.2005.1631619.

33. Lata S, Yadav S, Sohal A. Comparative study of different selection techniques in genetic algorithm. Internat J Engrg Sci. 2017.

34. IEEE Standard for Floating-Point Arithmetic. IEEE Std 754-2019 (Revision of IEEE 754-2008). 2019. p. 1-84. https://doi.org/10.1109/IEEESTD.2019.8766229.

35. Whitley D. A genetic algorithm tutorial. Stat Comput. 1998;4. https://doi.org/10.1007/BF00175354.

36. Bhardwaj M, Subharmanya B. PV inverter design using solar explorer kit. Available from: http://www.ti.com/lit/an/sprabr4a/sprabr4a.pdf.

37. Meddour S, Rahem D, Wira P, Laib H, Cherif AY, Chtouki I, et al. Design and implementation of an improved metaheuristic algorithm for maximum power point tracking algorithm based on a PV emulator and a double-stage grid-connected system. Eur J Electr Eng/Rev Int Génie Electr. 2022;24(3).

© 2024 The Author(s). | Published by Institute of Smart Energy Systems Press